THE MOTION TRAJECTORY-BASED FINITE-TIME CONTROL FOR THE MARINE SURFACE VEHICLE

(DOI No: 10.3940/rina.ijme.2020.a1.586)

H L Chen, **H X Ren**, **B C Yang** Dalian Maritime University, China and **J T Chen**, Qingdao Ocean Shipping Mariners College, China

SUMMARY

This brief is devoted to the predesigned motion trajectory-based finite time dynamic positioning (DP) control for a marine surface vehicle (MSV) with unknown external disturbances. Firstly, a preset motion trajectory is presented through establishing the relationship function among position tracking errors and heading tracking error, facilitating the MSV to arrive in the equilibrium point along the pre-designed trajectory. Furthermore, a novel nonsingular and fast terminal sliding mode control (NTSMC) approach is investigated, which ensures faster convergence rate and better stability performance of the close-loop system than the conventional backstepping control approach. What's more, by incorporating the adaptive technique with the NTSMC approach, an adaptive nonsingular and fast terminal sliding mode control (ANTSMC) strategy is addressed. Compared to the NTSMC approach, it strengthens robustness to disturbances and guarantees system states to converge to a closer neighborhood of the equilibrium point. Finally, simulation results illustrate the remarkable effectiveness of proposed control schemes.

NOMENCLATURE

x	Longitudinal position point (m)
y	Horizontal position point (m)
ψ	Heading (rad)
u	Longitudinal velocity (m/s)
v	Horizontal velocity (m/s)
r	Yawing angular velocity (rad/s)
MSV	Marine Surface Vehicle
NTSMC	Nonsingular and fast terminal sliding mode control
ANTSMC	Adaptive non-singular and fast terminal sliding mode control

1. INTRODUCTION

The dynamic positioning (DP) technology allows a ship to maintain its own position and heading at a fixed location or navigate along a predetermined track exclusively in a way that its own propulsion system counteracts environmental disturbances inducted by waves, currents, and wind (Fossen, & Grovlen, 1998). Compared with traditional anchor mooring positioning, the DP technology has a lot of advantages inclusive of easy operation, high positioning accuracy and avoidance of destroying riverbed, and it has been extensively applied in offshore operations such as wreck investigation, underwater cable laying, and oil drilling (Du *et al*, 2014). Therefore, it is increasingly essential for undertaking of relevant researches of DP technology.

As for DP control issues, nonlinear control methodologies such as backstepping control, sliding mode control, and mode predictive control nowadays have been playing a dominant position instead of previous linear control schemes of PID control and optimal control. Among them, correlational researches for backstepping control approach were practically active. More excitingly, abundant theoretical and experimental results are accomplished. In (Fossen, & Grovlen, 1998), a vector backstepping technique-based nonlinear control scheme was addressed, achieving a globally uniform asymptotic stability. Based on the control method (Fossen, & Grovlen, 1998), dynamic surface control (DSC) and adaptive technique were incorporated in (Du *et al*, 2014) to solve the problem of "explosion of complexity" and suppress unknown time-varying disturbances. In (Zhang *et al,* 2017) "minimal learning parameter" technique was originally introduced into backstepping algorithm, and the on-line learning parameters were reduced substantially, lowering the computational burden. As for the output feedback case, a backstepping method-based output feedback control law was given, and an adaptive observer was deducted to estimate the speed of the vessel and unknown parameters (Do, 2007). In (Du *et al,* 2015), supposing unknown of the vessel position, heading and speed, an output feedback controller coupling with a high-gain observer was presented, and the consequent simulation results were satisfying.

Nevertheless, overviewing the aforementioned research works, we observe two questions: on one hand, although the backstepping technique-based control approach assists to get good simulation results, the motion trajectory of MSV has never been involved in the past. In fact, we usually hope that the MSV should perform the DP task along a pre-planned trajectory that is satisfying to the practical requirement. On the other hand, the forgoing control methodologies can all achieve the exponential convergence and the tracking errors of closed-loop system were made asymptotically stable or globally uniformly ultimately bounded (GUUB) in infinite time. Whereas, in view of the practical engineering application, it is valuable that tracking errors are stable as early as possible in finite settling time. The finite-time control algorithm (Bhat & Bernstein 1997-Bhat & Bernstein, 2002) was proposed with the advantage of finite-time convergence as well as the interference rejection, and then it was successfully applied in a variety of engineering areas, such as underwater robot, mechanical arm and spacecraft attitude. Unfortunately, there are several literatures on applying the valuable method in DP control of MSV until now. In (Huang, 2018), based on the finite-time Lyapunov theory, an adaptive backstepping DP control was addressed, and model uncertainties and the disturbance upper bound were compensated by utilizing Radial Basis Function (RBF) network. In (Zhang, 2018), a nonsingular backstepping terminal sliding mode control approach was given, incorporating backstepping method and terminal sliding mode method.

In allusion of two issues, we propose a motion trajectory-based finite-time DP control scheme. Inspired by the design method in [30], a motion trajectory is firstly put forward. Next, referring to the design of terminal sliding mode in (Zhu *et al,* 2016), a NTSMC algorithm is proposed. It certifies that the proposed algorithm guarantees faster convergence characteristic and higher tracking accuracy, comparing to conventional asymptotic stability control algorithm. In addition, an adaptive method combined with the NTSMC algorithm is applied in estimating the upper bound of unknown disturbances, which can strengthen robustness to disturbances of the closed-loop system in further, guaranteeing system states to converge to a closer neighborhood of the equilibrium point.

2. PRELIMINARIES AND PROBLEM FORMULATION

2.1 PRELIMINARIES

Consider the nonlinear system:

$$\dot{\boldsymbol{x}} = \boldsymbol{f}(\boldsymbol{x},\boldsymbol{u}), \boldsymbol{x} \in \mathbb{R}^n \tag{1}$$

where $\boldsymbol{x}$ is the state vector, $\boldsymbol{u}$ is control input, $\boldsymbol{f}(\bullet)\text{:}\mathbb{R}^n \to \mathbb{R}^n$ is a continuous function, and $\boldsymbol{f}(0) = 0$. Suppose there exists a time function $T(\boldsymbol{x})$, and the time $t \geq T(\boldsymbol{x})$, satisfying $\boldsymbol{x}(t) = 0$, then the system (1) is finite-time stable[Wang *et al,* 2009].

If for any $\boldsymbol{x}(t_0) = \boldsymbol{x}_0$, there exists $T(\varepsilon, \boldsymbol{x}) < \infty$, such that $\|\boldsymbol{x}(t)\| < \varepsilon$, for all $t > t_0 + T$, and the nonlinear system is the practical finite-time stable (PFS).

Lemma 1: considering the system (1), suppose there exists a continuous definite function $V(\boldsymbol{x})$, such that $\dot{V}(\boldsymbol{x}) \leq -\mathrm{c}V^a(\boldsymbol{x})$ for some $c > 0, 0 < a < 1$, then the system (1) is finite-time stable [18] and the finite-time T satisfies

$$T_{reach} \leq \frac{V^{1-a}(x_0)}{c(1-a)} \tag{2}$$

where $V(\boldsymbol{x}_0)$ is the initial value of $V(\boldsymbol{x})$.

Lemma 2: considering the system (1), suppose there exists a continuous definite function $V(\boldsymbol{x})$, such that $\dot{V}(\boldsymbol{x}) \leq -\mathrm{c}V^a(\boldsymbol{x}) + \zeta$ for some $\lambda > 0, 0 < a < 1$ and $0 < \zeta < \infty$. Then the system (1) is practical finite-time stable (PFS)[19] and the finite-time satisfies

$$T_{reach} \leq \frac{V^{1-a}(x_0)}{c\theta_0(1-a)} \tag{3}$$

where $0 < \theta \leq 1$, and $V(\boldsymbol{x}_0)$ is the initial value of $V(\boldsymbol{x})$.

Lemma 3: if any $x_i, i = 1, 2, \cdots, n$, and $r \in (0,1)$, the following inequalities hold[20]:

$$\sum_{i=1}^{n} |x_i|^{1+r} \geq (\sum_{i=1}^{n} |x_i|^2)^{\frac{1+r}{2}} \tag{4}$$

Lemma 4: for any $a \in \mathbb{R}, b \in \mathbb{R}, p \geq 1$ is a constant, the following inequalities hold[Qian & Li, 2006]:

$$|a+b|^p \leq 2^{p-1}\left|a^p + b^p\right|, (|a|+|b|)^{1/p} \leq |a|^{1/p} + |b|^{1/p} \tag{5}$$

Lemma 5: for c, d and any real-valued function $\gamma(x, y) > 0$, the inequalities hold[Qian & Lin, 2015]:

$$|x|^c |y|^d \leq \frac{c}{c+d}\gamma(x,y)|x|^{c+d} + \frac{d}{c+d}\gamma(x,y)^{-c/d}|y|^{c+d} \tag{6}$$

Assumption 1: $\boldsymbol{\tau}_w = \left[\tau_{wu}, \tau_{wv}, \tau_{wr}\right]^{\mathrm{T}}$ is the unknown external disturbance (wind, wave), satisfying $|\boldsymbol{\tau}_w| \leq \boldsymbol{\tau}_w^* < \infty, \boldsymbol{\tau}_w^* = \left[\tau_{wu}^*, \tau_{wv}^*, \tau_{wr}^*\right]^{\mathrm{T}}$ is the upper bound, which is unknown vector, only for analysis.

2.2 DYNAMIC MODEL OF MSV

When analysing the motion of MSV in three DOF (degree of freedom), we need to establish two coordinate frames as shown in Figure. 1.

The earth-fixed reference frame X_0OY_0 is considered to be inertial, with OX_0 -axis pointing to north and OY_0 -axis pointing to east. $\boldsymbol{\eta} = \left[x, y, \psi\right]^{\mathrm{T}}$ is expressed as the 3 DOF position (x, y) and heading angle (ψ) of the vessel in this inertial frame. Besides, the body-fixed frame XAY is attached to the vessel with its origin A coincident with the centre of gravity. The AX-axis points to head of the vessel, and the AY-axis is perpendicular to the AX-axis and points to starboard side. Let $\boldsymbol{\upsilon}=[u,v,r]^{\mathrm{T}}$ be the corresponding velocity in surge, sway and yaw, respectively in the body-fixed frame.

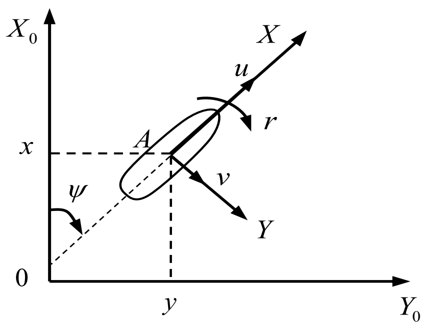

Figure. 1. Earth-fixed and body-fixed reference frames

The vectorial model of MSV is expressed as [Fossen 2002]

$$\dot{\boldsymbol{\eta}}=\boldsymbol{R}(\psi)\boldsymbol{\upsilon} \tag{7}$$

$$\boldsymbol{M}\dot{\boldsymbol{\upsilon}}+\boldsymbol{D}(\boldsymbol{\upsilon})\boldsymbol{\upsilon}=\boldsymbol{\tau}_{\upsilon}+\boldsymbol{\tau}_{w}+\boldsymbol{\omega}_{b} \tag{8}$$

$$\boldsymbol{\eta}_{output}=\boldsymbol{\eta}+\boldsymbol{\omega}_{\eta} \tag{9}$$

$$\boldsymbol{R}(\psi)=\begin{bmatrix}\cos\psi & -\sin\psi & 0\\ \sin\psi & \cos\psi & 0\\ 0 & 0 & 1\end{bmatrix} \tag{10}$$

$$\boldsymbol{M}=\begin{bmatrix}m-X_{\dot{u}} & 0 & 0\\ 0 & m-Y_{\dot{v}} & mx_G-Y_{\dot{r}}\\ 0 & mx_G-Y_{\dot{r}} & I_z-N_{\dot{r}}\end{bmatrix} \tag{11}$$

$$\boldsymbol{D}(\boldsymbol{\upsilon})\boldsymbol{\upsilon}=\begin{bmatrix}-X_u u-X_{|u|u}|u|u+Y_{\dot{v}}vr+Y_{\dot{r}}rr\\ -X_{\dot{u}}ur-Y_v v-Y_r r-Y_{|v|v}|v|v-Y_{|v|r}|v|r\\ (X_{\dot{u}}-Y_{\dot{v}})uv-Y_{\dot{r}}uv-N_v v-N_r r-N_{|v|v}|v|v-N_{|v|r}|v|r\end{bmatrix} \tag{12}$$

where $\boldsymbol{R}(\psi)$ denotes the velocity transformation matrix. $\boldsymbol{\tau}_{\upsilon}=[\tau_u,\tau_v,\tau_r]^{\mathrm{T}}$ is the effective control input, $\boldsymbol{\tau}_{w}=[\tau_{wu},\tau_{wv},\tau_{wr}]^{\mathrm{T}}$ is external disturbance induced by waves, wind. $\boldsymbol{M}$ is inertia matrix which includes hydrodynamic additional mass. It is symmetric positive definite, i.e., $\boldsymbol{M}=\boldsymbol{M}^T>0$. m and I_z are mass of the MSV, moment of inertia, while $Y_{\dot{v}},Y_{\dot{r}}$ and $N_{\dot{r}}$ denote added mass and added moment of inertia. The expression $\boldsymbol{D}(\boldsymbol{\upsilon})\boldsymbol{\upsilon}$ that consists of the Coriolis and centripetal force/moment and the nonlinear damping ones is the nonlinear hydrodynamic function. $X_u,X_{|u|u},Y_{\dot{v}},N_{\dot{v}}$, etc., denote the corresponding hydrodynamic derivatives. $\boldsymbol{\omega}_b\in\mathbb{R}^3$ and $\boldsymbol{\omega}_{\eta}\in\mathbb{R}^3$ are process noise vectors and measurement noise vector, respectively.

Actually, the abovementioned vectorial model, i.e., equations (7), (8) and (9), is the simulation model. In fact, according to the purpose of the controller design in this brief, the following design vectorial model is chosen, in which we replace nonlinear function $\boldsymbol{D}(\boldsymbol{\upsilon})\boldsymbol{\upsilon}$ with the linear hydrodynamic function $\boldsymbol{D}\boldsymbol{\upsilon}$ and ignore the process noise vector and measurement noise vector.

$$\dot{\boldsymbol{\eta}}=\boldsymbol{R}(\psi)\boldsymbol{\upsilon} \tag{13}$$

$$\boldsymbol{M}\dot{\boldsymbol{\upsilon}}+\boldsymbol{D}\boldsymbol{\upsilon}=\boldsymbol{\tau}_{\upsilon}+\boldsymbol{\tau}_{w} \tag{14}$$

$$\boldsymbol{D}\boldsymbol{\upsilon}=\begin{bmatrix}-X_u u\\ -Y_v v-X_{\dot{u}}r\\ -N_v v-N_r r\end{bmatrix} \tag{15}$$

2.3 MOTION TRAJECTORY DESIGN

Here, a motion trajectory generating method is given, by establishing a relationship function among position tracking errors η_{e1},η_{e2} and heading error η_{e3} .

$$\boldsymbol{\eta}_e=\boldsymbol{\eta}-\boldsymbol{\eta}_r$$

where $\boldsymbol{\eta}_e=[\eta_{e1},\eta_{e2},\eta_{e3}]^{\mathrm{T}}$ is tracking error vector, $\boldsymbol{\eta}_r=[x_r,\mathrm{y}_r,\psi_r]^{\mathrm{T}}$ is the reference tracking attitude.

$\eta_{e1}=x-x_r,\eta_{e2}=y-y_r,\eta_{e3}=\psi-\psi_r.$

Design the following relationship function

$$h=\frac{180}{\pi}\eta_{e3}+\eta_{e2}-\eta_{e1}$$

The projection of h within xy plane is $h_1=\eta_{e2}-\eta_{e1}$, while, the projection of h within $x\psi$ plane is $h_2=\eta_{e3}-\frac{\pi}{180}\eta_{e1}$.

When $h_1=h_2=0, y=x-x_r+y_r,\psi=\frac{\pi}{180}(x-x_r)+\psi_r$.

2.4 CONTROLLER DESIGN

In the kinematic design, a virtual control law is presented based on the backstepping technique; in the dynamic design, the virtual control law is regarded as the tracking target and a novel backstepping NTSMC approach is investigated.

Step 1: the deduction of virtual control law $\boldsymbol{a}_\upsilon$

Define the transforming tracking error and velocity error

$$\boldsymbol{\eta}_{eh} = [\eta_{e1}, h_1, h_2]^{\mathrm{T}} \tag{16}$$

$$\boldsymbol{\upsilon}_e = \boldsymbol{\upsilon} - \boldsymbol{a}_\upsilon \tag{17}$$

where $\boldsymbol{\eta}_{eh}$ is transforming tracking error, $\boldsymbol{\upsilon}_e$ is the velocity error, let $\boldsymbol{a}_\upsilon = -\boldsymbol{R}_h(\psi)^{-1}\boldsymbol{K}_1 Sig(\boldsymbol{\eta}_{eh})^a$ virtual control law.

Where

$$Sig(\boldsymbol{\eta}_{eh})^a = \begin{bmatrix} |\eta_{eh}(1)|^a \operatorname{sgn}(\eta_{eh}(1)) \\ |\eta_{eh}(2)|^a \operatorname{sgn}(\eta_{eh}(2)) \\ |\eta_{eh}(3)|^a \operatorname{sgn}(\eta_{eh}(3)) \end{bmatrix},$$

$$\boldsymbol{K}_1 = diag(k_{11}, k_{12}, k_{13}), 0 < a < 1$$

The derivative of (16)

$$\dot{\boldsymbol{\eta}}_{eh} = \left[\dot{\eta}_{e1}, \dot{h}_1, \dot{h}_2\right]^{\mathrm{T}} \tag{18}$$

$$\dot{h}_1 = \dot{y} - \dot{y}_r - \dot{\eta}_{e1} = (\sin\psi - \cos\psi)u + (\cos\psi + \sin\psi)v - \dot{y}_r + \dot{x}_r \tag{19}$$

$$\dot{h}_2 = \dot{\eta}_{e3} - \frac{\pi}{180}\dot{\eta}_{e1} = r - \frac{\pi}{180}(\cos\psi u - \sin\psi v) - \dot{\psi}_r + \frac{\pi}{180}\dot{x}_r \tag{20}$$

Substituting (19) and (20) into (18), obtain

$$\dot{\boldsymbol{\eta}}_{eh} = \begin{bmatrix} \cos\psi & -\sin\psi & 0 \\ \sin\psi - \cos\psi & \cos\psi + \sin\psi & 0 \\ -\frac{\pi}{180}\cos\psi & \frac{\pi}{180}\cos\psi & 1 \end{bmatrix} \begin{bmatrix} u \\ v \\ r \end{bmatrix} - \begin{bmatrix} \dot{x}_r \\ \dot{y}_r - \dot{x}_r \\ \dot{\psi}_r - \frac{\pi}{180}\dot{x}_r \end{bmatrix} \tag{21}$$

Let $\boldsymbol{R}_h(\psi) = \begin{bmatrix} \cos\psi & -\sin\psi & 0 \\ \sin\psi - \cos\psi & \cos\psi + \sin\psi & 0 \\ -\frac{\pi}{180}\cos\psi & \frac{\pi}{180}\sin\psi & 1 \end{bmatrix}$

$$\dot{\boldsymbol{\eta}}_{rh} = \begin{bmatrix} \dot{x}_r \\ \dot{y}_r - \dot{x}_r \\ \dot{\psi}_r - \frac{\pi}{180}\dot{x}_r \end{bmatrix}$$

$$\dot{\boldsymbol{\eta}}_{eh} = \boldsymbol{R}_h(\psi)\boldsymbol{\upsilon} - \dot{\boldsymbol{\eta}}_{rh} \tag{22}$$

Substituting (17) into (22) yields

$$\dot{\boldsymbol{\eta}}_{eh} = \boldsymbol{R}_h(\psi)\boldsymbol{a}_\upsilon + \boldsymbol{R}_h(\psi)\boldsymbol{\upsilon}_e - \dot{\boldsymbol{\eta}}_{rh} \tag{23}$$

Design the Lyapunov candidate

$$V_1 = \frac{1}{2}\boldsymbol{\eta}_{eh}^{\mathrm{T}}\boldsymbol{\eta}_{eh} \tag{24}$$

Time differentiation of V_1 gives

$$\dot{V}_1 = \boldsymbol{\eta}_{eh}^{\mathrm{T}}\left[\boldsymbol{R}_h(\psi)\boldsymbol{a}_\upsilon + \boldsymbol{R}_h(\psi)\boldsymbol{\upsilon}_e - \dot{\boldsymbol{\eta}}_{rh}\right] \tag{25}$$

Take the virtual control law $\boldsymbol{a}_\upsilon$, get

$$\dot{V}_1 = -\boldsymbol{\eta}_{eh}^{\mathrm{T}}\boldsymbol{K}_1 Sig(\boldsymbol{\eta}_{eh})^a + \boldsymbol{\eta}_{eh}^{\mathrm{T}}\boldsymbol{R}_h(\psi)\boldsymbol{\upsilon}_e \tag{26}$$

If $\boldsymbol{\upsilon}_e = 0, \dot{V}_1 = -\sum_{i=1}^{3} k_{1i}|\eta_{ehi}|^{1+a}$. According to Lemma 1, we can obtain

$$\dot{V}_1 = -\sum_{i=1}^{3} K_{1i}|\eta_{ehi}|^{1+a} \leq -2^{\frac{1+a}{2}}\lambda_{\min}(\boldsymbol{K}_1)V_1^{\frac{1+a}{2}}$$

Step 2: obtain the control $\boldsymbol{\tau}_{\mathrm{NTSMC}}$, when ignoring the external disturbances.

Refer to (Zhu *et al*, 2016), a non-singular and fast terminal sliding mode surface is designed.

$$\boldsymbol{s} = \boldsymbol{\upsilon}_e + \boldsymbol{d}_1\int_0^t \boldsymbol{\upsilon}_e d\tau + \boldsymbol{d}_2\int_0^t Sig(\boldsymbol{\upsilon}_e)^q d\tau \tag{27}$$

Design the NTSMC approach

$$\begin{aligned}\boldsymbol{\tau}_{\mathrm{NTSMC}} = {} & \boldsymbol{K}_2 Sig(\boldsymbol{s})^a + \boldsymbol{D}\boldsymbol{\upsilon} + \boldsymbol{M}\dot{\boldsymbol{a}}_\upsilon - \boldsymbol{M}\boldsymbol{d}_1\boldsymbol{\upsilon}_e - \boldsymbol{M}\boldsymbol{d}_2 Sig(\boldsymbol{\upsilon}_e)^q \\ & - \boldsymbol{s}^{-1}\boldsymbol{\eta}_{eh}^{\mathrm{T}}\boldsymbol{R}_h(\psi)\boldsymbol{\upsilon}_e\end{aligned} \tag{28}$$

where

$$Sig(\boldsymbol{\upsilon}_e)^q = \begin{bmatrix} |\upsilon_e(1)|^q \operatorname{sgn}(\upsilon_e(1)) \\ |\upsilon_e(2)|^q \operatorname{sgn}(\upsilon_e(2)) \\ |\upsilon_e(3)|^q \operatorname{sgn}(\upsilon_e(3)) \end{bmatrix}, 0.5 < q < 1,$$

$$\boldsymbol{d}_1 = diag(d_{11}, d_{12}, d_{13}), \boldsymbol{d}_2 = diag(d_{21}, d_{22}, d_{23}),$$
$$\boldsymbol{K}_2 = diag(k_{21}, k_{22}, k_{23})$$

Design the Lyapunov candidate

$$V_2 = V_1 + \frac{1}{2}\boldsymbol{s}^{\mathrm{T}}\boldsymbol{M}\boldsymbol{s}$$

The derivative of V_2 along with (26) and (27)

$$\begin{aligned}\dot{V}_2 = {} & \dot{V}_1 + \boldsymbol{s}^{\mathrm{T}}\boldsymbol{M}\dot{\boldsymbol{s}} = -\boldsymbol{\eta}_{eh}^{\mathrm{T}}\boldsymbol{K}_1 Sig(\boldsymbol{\eta}_{eh})^a + \boldsymbol{\eta}_{eh}^{\mathrm{T}}\boldsymbol{R}_h(\psi)\boldsymbol{\upsilon}_e \\ & - \boldsymbol{s}^{\mathrm{T}}\boldsymbol{M}(\dot{\boldsymbol{\upsilon}}_e + \boldsymbol{d}_1\boldsymbol{\upsilon}_e + \boldsymbol{d}_2 \operatorname{Sig}(\boldsymbol{\upsilon}_e)^q)\end{aligned} \tag{29}$$

Substituting $\boldsymbol{\tau}_{\mathrm{NTSMC}}$ into (29) yields

$$\begin{aligned}\dot{V}_2 &= -\boldsymbol{\eta}_{eh}^{\mathrm{T}}\boldsymbol{K}_1 Sig(\boldsymbol{\eta}_{eh})^a - \boldsymbol{s}^{\mathrm{T}}\boldsymbol{K}_2 Sig(\boldsymbol{s})^a \\ &\le -2^{\frac{1+a}{2}}\lambda_{\min}(\boldsymbol{K}_1)V_1^{\frac{1+a}{2}} - 2^{\frac{1+a}{2}}\frac{\lambda_{\min}(\boldsymbol{K}_2)}{\lambda_{\max}(\boldsymbol{M})^{\frac{1+a}{2}}}\left(\frac{1}{2}\boldsymbol{s}^{\mathrm{T}}\boldsymbol{M}\boldsymbol{s}\right)^{\frac{1+a}{2}} \\ &\le -mV_2^{\frac{1+a}{2}}\end{aligned}$$

where $m = 2^{\frac{1+a}{2}}\min\left\{\lambda_{\min}(\boldsymbol{K}_1), \frac{\lambda_{\min}(\boldsymbol{K}_2)}{\lambda_{\max}(\boldsymbol{M})^{\frac{1+a}{2}}}\right\}$

$\lambda_{\min}(\bullet)$ is the minimum eigenvalue of a matrix and $\lambda_{\max}(\bullet)$ is the maximum eigenvalue of a matrix.

According to Lemma 1, and the closed-loop system is finite time stable under the condition of ignoring external disturbances. And the tracking errors will converge to the equilibrium point in finite time

$$T_{reach} \le \frac{V_2^{\frac{1+a}{2}}(\boldsymbol{x}(0))}{m(1-\frac{1+a}{2})}$$

Step 3: obtain the practical ANTSMC strategy $\boldsymbol{\tau}_{\mathrm{ANTSMC}}$

$$\boldsymbol{\tau}_{\mathrm{ANTSMC}} = \boldsymbol{\tau}_{\mathrm{NTSMC}} - \hat{\boldsymbol{\tau}}_w^* \tag{30}$$

where $\boldsymbol{\tau}_{\mathrm{NTSMC}}$ is the control scheme in (28), $\hat{\boldsymbol{\tau}}_w^* = \left[\hat{\tau}_{wu}^*, \hat{\tau}_{wv}^*, \hat{\tau}_{wr}^*\right]^{\mathrm{T}}$ is the upper bound estimated vector of disturbances, and the adaptive law

$$\dot{\hat{\boldsymbol{\tau}}}_w^* = \boldsymbol{K}_3\left[\vartheta\boldsymbol{s} - \boldsymbol{K}_4(\hat{\boldsymbol{\tau}}_w^* - \boldsymbol{\tau}_w^0)\right] \tag{31}$$

$\vartheta = diag(\tanh(\frac{s(1)}{\varepsilon_1}), \tanh(\frac{s(2)}{\varepsilon_2}), \tanh(\frac{s(3)}{\varepsilon_3})),$

$\boldsymbol{K}_3 = diag(k_{31}, k_{32}, k_{33}), \boldsymbol{K}_4 = diag(k_{41}, k_{42}, k_{43}), \varepsilon_1, \varepsilon_2, \varepsilon_3$ are design parameters.

$\tilde{\boldsymbol{\tau}}_w^* = \hat{\boldsymbol{\tau}}_w^* - \boldsymbol{\tau}_w^*$ is estimating error vector, $\boldsymbol{\tau}_w^*$ is upper bound vector of external disturbances, $\boldsymbol{\tau}_w^0 = \left[\tau_{wu}^0, \tau_{wv}^0, \tau_{wr}^0\right]^{\mathrm{T}}$ is the design constant vector.

Design the Lyapunov candidate

$$V_3 = V_1 + \frac{1}{2}\boldsymbol{s}^{\mathrm{T}}\boldsymbol{M}\boldsymbol{s} + \frac{1}{2}\tilde{\boldsymbol{\tau}}_w^{*\mathrm{T}}\boldsymbol{K}_3^{-1}\tilde{\boldsymbol{\tau}}_w^* \tag{32}$$

Derivate V_3 along with (26) and (27)

$$\begin{aligned}\dot{V}_3 &= \dot{V}_1 + \boldsymbol{s}^{\mathrm{T}}\boldsymbol{M}\dot{\boldsymbol{s}} + \tilde{\boldsymbol{\tau}}_w^{*\mathrm{T}}\boldsymbol{K}_3^{-1}\dot{\hat{\boldsymbol{\tau}}}_w^* = -\boldsymbol{\eta}_{eh}^{\mathrm{T}}\boldsymbol{K}_1 Sig(\boldsymbol{\eta}_{eh})^a - \\ &\boldsymbol{s}^{\mathrm{T}}\boldsymbol{K}_2 Sig(\boldsymbol{s})^a + \sum_{i=1}^{3}|s(i)|\tau_w^*(i) - \boldsymbol{s}^{\mathrm{T}}\vartheta\boldsymbol{\tau}_w^* - \tilde{\boldsymbol{\tau}}_w^{*\mathrm{T}}\boldsymbol{K}_4(\hat{\boldsymbol{\tau}}_w^* - \boldsymbol{\tau}_w^0)\end{aligned} \tag{33}$$

According to Assumption 1, and substituting (14), (17), (28) and (31) into (33) yields

$$\begin{aligned}\dot{V}_3 &= \dot{V}_1 + \boldsymbol{s}^{\mathrm{T}}\boldsymbol{M}\dot{\boldsymbol{s}} + \tilde{\boldsymbol{\tau}}_w^{*\mathrm{T}}\boldsymbol{K}_3^{-1}\dot{\hat{\boldsymbol{\tau}}}_w^* = -\boldsymbol{\eta}_{eh}^{\mathrm{T}}\boldsymbol{K}_1 Sig(\boldsymbol{\eta}_{eh})^a - \boldsymbol{s}^{\mathrm{T}}\boldsymbol{K}_2 Sig(\boldsymbol{s})^a \\ &+ \sum_{i=1}^{3}|s(i)|\tau_w^*(i) - \boldsymbol{s}^{\mathrm{T}}\vartheta\boldsymbol{\tau}_w^* - \tilde{\boldsymbol{\tau}}_w^{*\mathrm{T}}\boldsymbol{K}_4(\hat{\boldsymbol{\tau}}_w^* - \boldsymbol{\tau}_w^0)\end{aligned} \tag{34}$$

Applying hyperbolic tangent function $\tanh(\bullet)$, and for any $\varsigma > 0, a \in \mathbb{R}$, get

$$0 \le |a| - a\tanh(\frac{a}{\varsigma}) \le \beta\varsigma$$

where β is a constant, satisfying $\beta = e^{-(\beta+1)}, \beta = 0.2785.$

$$\begin{aligned}\dot{V}_3 &= \dot{V}_1 + \boldsymbol{s}^{\mathrm{T}}\boldsymbol{M}\dot{\boldsymbol{s}} + \tilde{\boldsymbol{\tau}}_w^{*\mathrm{T}}\boldsymbol{K}_3^{-1}\dot{\hat{\boldsymbol{\tau}}}_w^* = -\boldsymbol{\eta}_{eh}^{\mathrm{T}}\boldsymbol{K}_1 Sig(\boldsymbol{\eta}_{eh})^a - \boldsymbol{s}^{\mathrm{T}}\boldsymbol{K}_2 Sig(\boldsymbol{s})^a \\ &- \tilde{\boldsymbol{\tau}}_w^{*\mathrm{T}}\boldsymbol{K}_4(\hat{\boldsymbol{\tau}}_w^* - \boldsymbol{\tau}_w^0) + 0.2785\boldsymbol{E}^{\mathrm{T}}\tau_w^*.\end{aligned}$$

where $\boldsymbol{E} = \left[\varepsilon_1, \varepsilon_2, \varepsilon_3\right]^{\mathrm{T}}$.

$$\begin{aligned}\dot{V}_3 &\le -2^{\frac{1+a}{2}}\lambda_{\min}(\boldsymbol{K}_1)V_1^{\frac{1+a}{2}} - 2^{\frac{1+a}{2}}\frac{\lambda_{\min}(\boldsymbol{K}_2)}{\lambda_{\max}(\boldsymbol{M})^{\frac{1+a}{2}}}\left(\frac{1}{2}\boldsymbol{s}^{\mathrm{T}}\boldsymbol{M}\boldsymbol{s}\right)^{\frac{1+a}{2}} \\ &- \tilde{\boldsymbol{\tau}}_w^{*\mathrm{T}}\boldsymbol{K}_4(\hat{\boldsymbol{\tau}}_w^* - \boldsymbol{\tau}_w^0) + 0.2785\boldsymbol{E}^{\mathrm{T}}\tau_w^* \\ &\le -mV_2^{\frac{1+a}{2}} - \tilde{\boldsymbol{\tau}}_w^{*\mathrm{T}}\boldsymbol{K}_4(\hat{\boldsymbol{\tau}}_w^* - \boldsymbol{\tau}_w^0) + 0.2785\boldsymbol{E}^{\mathrm{T}}\tau_w^*\end{aligned} \tag{35}$$

Adopting $n = \frac{1+a}{2}, V_3^n = (V_1 + \frac{1}{2}\boldsymbol{s}^{\mathrm{T}}\boldsymbol{M}\boldsymbol{s} + \frac{1}{2}\tilde{\boldsymbol{\tau}}_w^{*\mathrm{T}}\boldsymbol{K}_3^{-1}\tilde{\boldsymbol{\tau}}_w^*)^n$

According to lemma 4, yields

$$V_3^n \le V_1^n + (\frac{1}{2}\boldsymbol{s}^{\mathrm{T}}\boldsymbol{M}\boldsymbol{s})^n + (\frac{1}{2}\tilde{\boldsymbol{\tau}}_w^{*\mathrm{T}}\boldsymbol{K}_3^{-1}\tilde{\boldsymbol{\tau}}_w^*)^n \tag{36}$$

According to (35) and (36), get

$$\begin{aligned}\dot{V}_3 &\le -mV_3^{\frac{1+a}{2}} + m(\frac{1}{2}\tilde{\boldsymbol{\tau}}_w^{*\mathrm{T}}\boldsymbol{K}_3^{-1}\tilde{\boldsymbol{\tau}}_w^*)^n - \tilde{\boldsymbol{\tau}}_w^{*\mathrm{T}}\boldsymbol{K}_4(\hat{\boldsymbol{\tau}}_w^* - \boldsymbol{\tau}_w^0) \\ &+ 0.2785\boldsymbol{E}^{\mathrm{T}}\tau_w^*\end{aligned} \tag{37}$$

According to Lemma 5, obtain

$$m(\frac{1}{2}\tilde{\boldsymbol{\tau}}_w^{*\mathrm{T}}\boldsymbol{K}_3^{-1}\tilde{\boldsymbol{\tau}}_w^*)^n \le \frac{1}{2}\tilde{\boldsymbol{\tau}}_w^{*\mathrm{T}}\boldsymbol{K}_3^{-1}\tilde{\boldsymbol{\tau}}_w^* + (1-n)n^{n/(1-n)}m^{1/(1-n)}$$

$$\dot{V}_3 \le -mV_3^{\frac{1+a}{2}} + m\left(\frac{1}{2}\tilde{\boldsymbol{\tau}}_w^{*\mathrm{T}}\boldsymbol{K}_3^{-1}\tilde{\boldsymbol{\tau}}_w^{*}\right)^n \le \frac{1}{2}\tilde{\boldsymbol{\tau}}_w^{*\mathrm{T}}\boldsymbol{K}_3^{-1}\tilde{\boldsymbol{\tau}}_w^{*} + (1-n)n^{n/(1-n)}m^{1/(1-n)}$$
$$-\frac{1}{2}\tilde{\boldsymbol{\tau}}_w^{*\mathrm{T}}\boldsymbol{K}_4\tilde{\boldsymbol{\tau}}_w^{*} + \frac{1}{2}(\hat{\boldsymbol{\tau}}_w^{*}-\boldsymbol{\tau}_w^{0})^{\mathrm{T}}\boldsymbol{K}_4(\hat{\boldsymbol{\tau}}_w^{*}-\boldsymbol{\tau}_w^{0}) + 0.2785\boldsymbol{E}^{\mathrm{T}}\tau_w^{*} \tag{38}$$

$$\dot{V}_3 \le -mV_3^{\frac{1+a}{2}} - \frac{1}{2}\tilde{\boldsymbol{\tau}}_w^{*\mathrm{T}}(\boldsymbol{K}_4-\boldsymbol{K}_3^{-1})\tilde{\boldsymbol{\tau}}_w^{*} + (1-n)n^{n/(1-n)}m^{1/(1-n)}$$
$$+\frac{1}{2}(\hat{\boldsymbol{\tau}}_w^{*}-\boldsymbol{\tau}_w^{0})^{\mathrm{T}}\boldsymbol{K}_4(\hat{\boldsymbol{\tau}}_w^{*}-\boldsymbol{\tau}_w^{0}) + 0.2785\boldsymbol{E}^{\mathrm{T}}\tau_w^{*} \tag{39}$$

Choose $\boldsymbol{K}_4$ and $\boldsymbol{K}_3^{-1}$ appropriately to make sure $\boldsymbol{K}_4-\boldsymbol{K}_3^{-1}\ge 0$, so

$$\dot{V}_3 \le -mV_3^n + \delta \tag{40}$$

$$\delta = (1-n)n^{n/(1-n)}m^{1/(1-n)} + \frac{1}{2}(\hat{\boldsymbol{\tau}}_w^{*}-\boldsymbol{\tau}_w^{0})^{\mathrm{T}}\boldsymbol{K}_4(\hat{\boldsymbol{\tau}}_w^{*}-\boldsymbol{\tau}_w^{0}) + 0.2785\boldsymbol{E}^{\mathrm{T}}\tau_w^{*}$$

According to Lemma 2, the error signals of close-loop system converge to the following stability domain $V_3 \le \left(\frac{\delta}{m(1-\theta_0)}\right)^{\frac{2}{1+a}}$ in finite time $T \le \frac{V_3^{1-a}(V_3(\boldsymbol{x}_0))}{m\theta_0(1-a)}$.

3. SIMULATION

In this section, one MSV model (Zhang *et al,* 2017) is selected as the plant and comparative experiments with the results in (Du *et al,* 2014) are illustrated in order to certify the performance of the proposed control algorithm.

The MSV model parameters are listed bellow

$$X_{\dot{u}} = -0.7212\times10^6, Y_{\dot{v}} = -3.6921\times10^6,$$
$$Y_{\dot{r}} = -1.0234\times10^6, I_z - N_{\dot{r}} = 3.7454\times10^9,$$
$$X_u = 5.0242\times10^4, Y_v = 2.7229\times10^5,$$
$$Y_r = -4.3933\times10^6, Y_{|v|v} = 1.7860\times10^4,$$
$$X_{|u|u} = 1.0179\times10^3, Y_{|v|r} = -3.0068\times10^5,$$
$$N_v = -4.3821\times10^6, N_r = 4.1894\times10^8,$$
$$N_{|v|v} = -2.4684\times10^5, N_{|v|r} = 6.5759\times10^6, m = 4.591\times10^6.$$

The initial position and heading of the MSV model is $\boldsymbol{\eta}(0)=[20m,20m,20^0]^{\mathrm{T}}$, the desired reference attitude is $\boldsymbol{\eta}_r=[0m,0m,0^0]^{\mathrm{T}}$. The other initial state is $\boldsymbol{\upsilon}(0)=[0m/s,0m/s,0^0/s]^{\mathrm{T}}$.

As to the external disturbances, the sea wind and irregular wind-generated wave are involved in simulations.

The wind speed is $V_{wind}=4m/s$, and wind direction is $\psi_{wind}=60\deg$.

The disturbance forces and moment, i.e., the wind forces and moment and 2nd-order wave forces and moment, are described as follows

$$\bar{X}_{wind} = \frac{1}{2}\rho_\alpha A_f U_R^2 C_{wx}(\alpha_R)$$
$$\bar{Y}_{wind} = \frac{1}{2}\rho_\alpha A_s U_R^2 C_{wy}(\alpha_R)$$
$$\bar{N}_{wind} = \frac{1}{2}\rho_\alpha A_s L_{oa} U_R^2 C_{wn}(\alpha_R)$$
$$X_{wave}^D = \rho L_{oa}\cos\chi\sum_{i=1}^{m} C_{Xw}^D(2\pi\omega_i^2/\mathrm{g})S_{\zeta\zeta}(\omega_i)\Delta\omega$$
$$Y_{wave}^D = \frac{1}{2}\rho L_{oa}\sin\chi\sum_{i=1}^{m} C_{Yw}^D(2\pi\omega_i^2/\mathrm{g})S_{\zeta\zeta}(\omega_i)\Delta\omega$$
$$N_{wave}^D = \frac{1}{2}\rho L_{oa}^2\sin\chi\sum_{i=1}^{m} C_{Nw}^D(2\pi\omega_i^2/\mathrm{g})S_{\zeta\zeta}(\omega_i)\Delta\omega$$
$$\boldsymbol{\tau}_w = [\tau_{wu},\tau_{wv},\tau_{wr}]^{\mathrm{T}}, \tau_{wu} = \bar{X}_{wind} + X_{wave}^D$$
$$\tau_{wv} = \bar{Y}_{wind} + Y_{wave}^D, \tau_{wr} = N_{wind} + N_{wave}^D$$

Please refer to the literature (Jia & Yang, 1999) to obtain specified meanings of disturbance model parameters in detail.

The controller parameters are all given

$$k_{11}=0.105, k_{12}=0.18, k_{13}=0.038,$$
$$k_{21}=7.3\times10^5, k_{22}=9.5\times10^5, k_{23}=9.5\times10^7,$$
$$k_{31}=9.3\times10^5, k_{32}=1.5\times10^6, k_{33}=2.0\times10^9,$$
$$k_{41}=7.3\times10^{-8}, k_{42}=8.3\times10^{-8}, k_{43}=1.6\times10^{-10},$$
$$d_{11}=0.09, d_{12}=0.1, d_{13}=0.01, d_{21}=0.1,$$
$$d_{22}=0.08, d_{23}=0.013, \varepsilon_1=0.2, \varepsilon_2=0.01, \varepsilon_3=0.01.$$

Simulation results are shown in Figures. 2-6. In addition, Tables 1-2 give the results of performance comparisons.

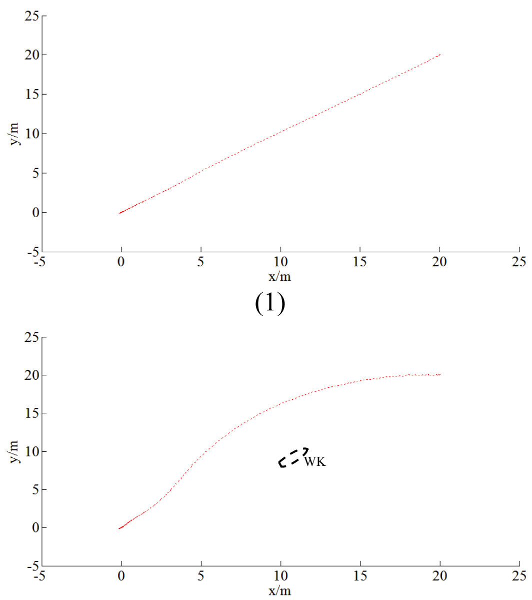

(2)

Figure. 2. Trajectory of MSV in *xy* plane

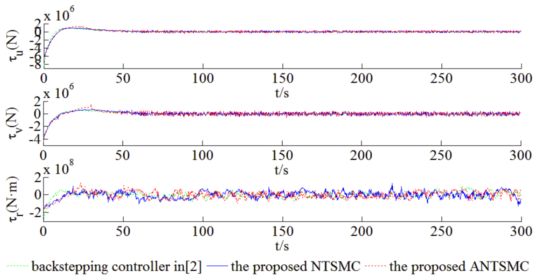

Figure. 3. Variation curves of control forces τ_u, τ_v and moment τ_r

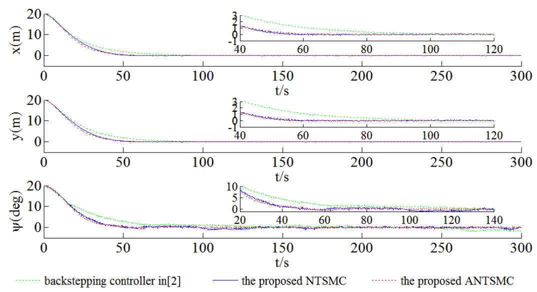

Figure. 4. Variation curves of actual position x, y and heading ψ

Table 1 Tracking error comparisons

Performance		Backstepping control in[2]	Proposed $\boldsymbol{\tau}_{\text{NTSMC}}$	Proposed $\boldsymbol{\tau}_{\text{ANTSMC}}$
	x_e(m)	1.5671	1.3125	1.2567
MAE	y_e(m)	1.6086	1.3174	1.2664
	ψ_e(deg)	2.2455	1.5424	1.4086

As showed in Figure. 2(1), the proposed adaptive control scheme $\boldsymbol{\tau}_{\text{ANTSMC}}$ is capable of overcoming influence of external disturbances, arrives smoothly along the straight-line motion trajectory ($y = x - x_r + y_r$) in xy plane and maintains the preset terminal position successfully at last. It is obviously the shortest distance between original position and terminal position with the advantage of saving time and energy. Of course, we can also devise other curve motion trajectories. For example, suppose that there is a wreck shown in Figure. 2(2) on the connection line between initial position and terminal position, we consider to design a curve motion trajectory in xy plane in Figure. 2(2). MSV is obviously able to reach the destination along the curve trajectory, avoiding colliding with the wreck.

Next, Figures. 3-4 demonstrate control inputs and the convergence trajectory comparisons of system states, i.e., x, y and ψ , in detail under three control methodologies ($\boldsymbol{\tau}_{\text{ANTSMC}}, \boldsymbol{\tau}_{\text{NTSMC}}$ and the backstepping control method) in detail. In Figure. 4, we can discern easily that the finite time control scheme $\boldsymbol{\tau}_{\text{NTSMC}}$ can achieve superior tracking performance in terms of rapid response, in comparison with backstepping control scheme in (Du *et al,* 2014). It means that the control scheme $\boldsymbol{\tau}_{\text{NTSMC}}$ ensures faster convergence rate of the closed-loop system than backstepping control scheme in (Du *et al,* 2014).

Moreover, the qualification analysis is summarized in Table 1, where the mean absolute error (MAE) is used to evaluate stability performance of three control algorithms. We can observe obviously that steady-state errors of x_e, y_e and ψ_e under the control scheme $\boldsymbol{\tau}_{\text{NTSMC}}$ reduce to 1.3125, 1.3174 and 1.5424, lowering by 16.2%, 18.1% and 31.3%, respectively in comparison with that under the backstepping control scheme in (Du *et al,* 2014). Results illustrate that the finite time control scheme $\boldsymbol{\tau}_{\text{NTSMC}}$ poses better stability performance.

What's more, as observed in Table 1, due to adaptive estimation of external disturbances, the control scheme $\boldsymbol{\tau}_{\text{ANTSMC}}$ further shrinks the steady-state errors, dropping to 1.2567, 1.2664 and 1.4086, respectively, compared to the controller $\boldsymbol{\tau}_{\text{NTSMC}}$. That proves that the control scheme $\boldsymbol{\tau}_{\text{ANTSMC}}$ guarantees steady-state errors to converge to the closest neighbourhood of the equilibrium point among three control algorithms.

Based on the analysis above, it is clear that the proposed finite time control scheme $\boldsymbol{\tau}_{\text{ANTSMC}}$ facilities the fastest convergence rate and best stability performance among three control algorithms.

In order to verify robustness superiority of the finite time control algorithm, we directly rise the wind speed from $4m/s$ to $12m/s$, and continue to carry out the other comparison simulations as shown in Figures. 5-6.

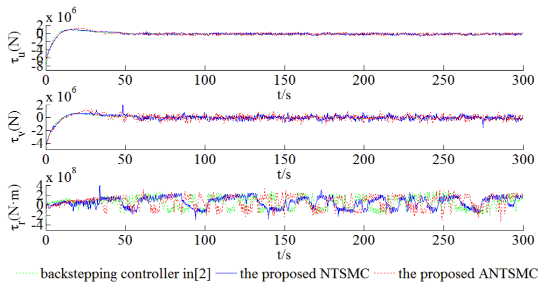

Figure. 5. Variation curves τ_u, τ_v and τ_r with $V_{wind} = 4m/s$

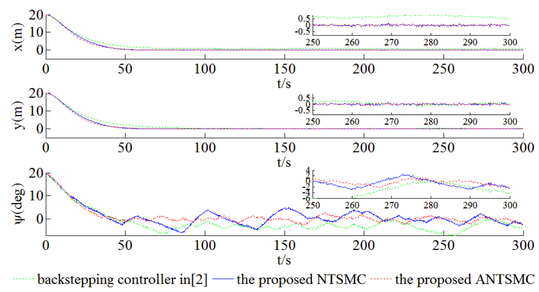

Figure. 6. Variation curves of x, y and ψ with $V_{wind} = 12m/s$

Table 2 Tracking error comparisons with $V_{wind} = 12m/s$

Performance		Backstepping control in[2]	Proposed $\boldsymbol{\tau}_{\text{NTSMC}}$	Proposed $\boldsymbol{\tau}_{\text{ANTSMC}}$
MAE	x_e(m)	2.1124	1.3230	1.2577
	y_e(m)	1.7613	1.3250	1.2674
	ψ_e(deg)	3.8383	2.6909	1.7475

According to disturbance model in this section, the rise of wind speed from $4m/s$ to $12m/s$ results in the strength of disturbance forces and moment. Therefore, we can see that the jitters of control inputs τ_u, τ_v and τ_r in Figure. 5 are stronger than that in Figure. 3 in order to sustain the stability of the close system.

As viewed in Figure. 6 and Table 2, we can see obviously that there is a relevant rise of steady-state errors, i.e., x_e, y_e and ψ_e, in comparison with that in Figure. 4 and Table 1, because of the growth of the disturbance forces and moment (wind and wave). Especially, as we can see, the steady-state errors under the backstepping control scheme climb to 2.1124, 1.7613 and 3.8383, respectively, increasing by 34.8%, 9.5% and 70.9%, respectively. Besides, there is a minor increase of steady-state errors under the control scheme $\boldsymbol{\tau}_{\text{NTSMC}}$. The error values go up to 1.3230, 1.3250 and 2.6909, respectively. However, they are still less than that under backstepping control scheme in (Du *et al,* 2014). In consequence, it proves that robustness to disturbances of the finite time control algorithm is better than the backstepping control algorithm. Furthermore, duo to the addition of disturbance compensation in the control scheme $\boldsymbol{\tau}_{\text{ANTSMC}}$, the steady-state errors under the control scheme $\boldsymbol{\tau}_{\text{ANTSMC}}$ stay the lowest, just increasing from 1.2567, 1.2664, and 1.4086 to 1.2577, 1.2674 and 1.7475, respectively.

Overall, all abovementioned simulation results and data comparison analysis testify that the finite time control algorithm finishes the advantages of faster convergence rate, better stability performance and more excellent robustness to disturbances, in comparison with the backstepping control algorithm.

Remark: the curve motion trajectory is implemented by the following method.

Design the following relationship function

$$h = \eta_{e3} + \eta_{e2} - 20\sin(\frac{\pi}{40}\eta_{e1})$$

The projection of h within xy plane is $h_1 = \eta_{e2} - 20\sin(\frac{\pi}{40}\eta_{e1})$. For the detail meanings of parameters, please refer to section 2.3.

4. CONCLUSION

In this brief, one NTSMC approach for DP control is originally derived based on a motion trajectory. The motion trajectory between initial point and the terminal point is established according to requirements of engineering application by designing a relationship function among position tracking errors η_{e1}, η_{e2} and heading error η_{e3}. Next, it demonstrates that the NTSMC approach not only raises the convergence rate of the closed-loop system, but also lower the state errors, compared with the conventional backstepping control approach. Furthermore, by employing adaptive technique and the NTSMC approach, we present an ANTSMC approach, which further strengthens robustness to disturbances, and decline steady-state errors to the lowest among three control algorithms. At last, finial simulation results certify remarkably outstanding performances of the ANTSMC approach in terms transient and steady-state responses.

5. REFERENCES

1. FOSSEN, T. & GROVLEN, Å. *Nonlinear output feedback control of dynamically positioned ships using vectorial observer backstepping*. IEEE Transactions on Control Systems Technology, 1998, 6(1):121-128. DOI: 10.1109/87.654882.
2. DU, J., *et al*. *Control law design of dynamic positioning for ship based on dynamic surface control*. Journal of Traffic & Transportation Engineering, 2014. DOI: 10.3969/j.issn.1671-1637.2014.05.005.
3. ZHANG, G., *et al*. *Robust Neural Control for Dynamic Positioning Ships with the Optimum-Seeking Guidance*. IEEE Transactions on Systems Man & Cybernetics Systems, 2017, 47(7):1500-1509. DOI: 10.1109/tsmc.2016.2628859.
4. DO, K. *Global Robust and Adaptive Output Feedback Dynamic Positioning of Surface Ships*. IEEE International Conference on Robotics and Automation. IEEE, 2007:4271-4276. DOI: 10.1007/s11804-011-1076-z.
5. DU, J., *et al*. *Adaptive Robust Output Feedback Control for a Marine Dynamic Positioning System Based on a High-Gain Observer*. IEEE Transactions on Neural Networks & Learning Systems, 2015, 26(11):2775-2786. DOI: 10.1109/TNNLS.2015.2396044.
6. BHAT, S & BERNSTEIN, D. *Finite-time stability of homogeneous systems*. American Control Conference, 1997. Proceedings of the. IEEE, 1997:2513-2514 Vol.4. DOI: 10.1109/ACC.1997.609245.
7. BHAT, S. & BERNSTEIN, D. *Continuous finite-time stabilization of the translational and rotational double integrators*. IEEE

Transactions on Automatic Control, 2002, 43(5):678-682. DOI: 10.1109/9.668834.

8. WANG, Y., *et al*. *Nonsingular Fast Terminal Sliding Mode Control for Underwater Vehicles*. Journal of Zhejiang University (Engineering), 2014, 48(9):1541-1551. DOI: 10.3785/j.issn.1008-97X.2014.09.001.
9. LI, S., *et al*. *Finite-Time Output Feedback Tracking Control for Autonomous Underwater Vehicles*. IEEE Journal of Oceanic Engineering, 2015, 40(3):727-751. DOI: 10.1109/JOE.2014.2330958.
10. HU, L., *et al*. *Nonsingular fast terminal sliding mode control method for 6-DOF manipulator*. Journal of Jilin University (Engineering), 2014, 44(3):735-741. DOI: 10.13229/j.cnki.jdxbgxb201403025.
11. VAN, M., *et al*. *An Adaptive backstepping nonsingular fast terminal sliding mode control for robust fault tolerant control of robot manipulators*. IEEE Transactions on Systems Man & Cybernetics Systems, 2019, 49(7):1448-1458. DOI: 10.1109/TSMC.2017.2782246.
12. SONG, S., *et al*. *Finite-time attitude tracking control for spacecraft with input saturation*. Journal of Control and Decision, 2015, 30(11):2004-2008. DOI: 10.13195/j.kzyjc.2014.1436.
13. LU, K., *et al*. *Finite-time tracking control of rigid spacecraft under actuator saturations and faults*. IEEE Transactions on Automation Science & Engineering, 2016, 13(1):368-381. DOI: 10.1049/iet-cta.2012.1031.
14. HUANG, C. *Finite-time dynamic positioning control for marine ships under the consideration of command propeller pitch*. Dalian: Dalian Maritime University, 2018.
15. ZHANG, G., *et al*. *Adaptive finite time dynamic positioning control of full-actuated ship with servo system uncertainties*. Journal of Automatica Sinica, 2018, 44(10): 1908 - 1912. DOI: 10.16383/j.aas.2017.c170111.
16. ZHU, Q., *et al*. *Adaptive finite time trajectory tracking for autonomous surface vehicle with unknown disturbance*. Journal of Systems Engineering and Electronics, 2016, 38(2):368-374. DOI: 10.3969/j.issn.1001-506X.2016.02.20.
17. WANG, L., *et al*. *Neural-network-based terminal sliding-mode control of robotic manipulators including actuator dynamics*. IEEE Transactions on Industrial Electronics, 2009, 56(9):3296-3304. DOI: 10.1109/TIE.2008.2011350.
18. BHAT, S. & BERNSTEIN, D. *Finite-time stability of continuous autonomous systems*. Society for Industrial and Applied Mathematics, 2000. DOI: 10.1137/S0363012997321358.
19. MU, C., *et al*. *Phase trajectory and transient analysis for nonsingular terminal sliding mode control systems*. Journal of Automatica Sinica, 2013, 39(6):902-908. DOI: CNKI.SUN.MOTO.0.2013-06-025.
20. BHAT, S. *Finite-time stability of continuous autonomous systems*. Siam J.contr. opti, 2000, 38(3):751-766. DOI: 10.1137/S0363012997321358.
21. QIAN, C. & LI, J. *Global output feedback stabilization of upper - triangular nonlinear systems using a homogeneous domination approach*. International Journal of Robust & Nonlinear Control, 2006, 16(9):441-463. DOI: 10.1109/ACC.2009.5160406.
22. QIAN, C. & LIN, W. *Non-Lipschitz continuous stabilizers for nonlinear systems with uncontrollable unstable linearization*. Systems & Control Letters, 2015, 42(3):185-200. DOI: 10.1002/rnc.1074.
23. FOSSEN, T. *Marine Control Systems: Guidance, Navigation, and Control of Ships, Rigs and Underwater Vehicles*. Marine Control System, Guidance, Navigation and Control of Ships, Rigs and Underwater. 2002. ISBN: 8292356002.
24. ALME, J. *Autotuned Dynamic Positioning for Marine Surface Vessels*. Department of Engineering Cybernetics, 2008.
25. JIA, X. & YANG, Y. (1999) *Mechanism modelling and identification modelling of ship motion mathematical mode.* Dalian maritime university press, Dalian. ISBN 7-5632-1137-3.